ELECTRONIC SUPPLEMENTARY INFORMATION

Table S1: Calorimetric characteristics of the transition in $[(CH_3)_2NH_2][Mn(HCOO)_3]$.

Heating/cooling rate (K/min)	**T_{max}(K)** heating/endo	**ΔH (J/mol)** heating/endo	**ΔS(J/molK)** heating/endo	**T_{max}(K)** cooling/exo	**$\Delta T_{heat-cool}$**	**ΔH (J/mol)** cooling/exo	**ΔS (J/molK)** cooling/exo
5	189.17	1671.6	8.83	182.55	6.62	1701.6	9.32
10	189.84	1679.4	8.84	181.65	8.19	1713.4	9.43
20	191.08	1667.9	8.73	180.16	10.92	1710.6	9.49

It should be noted that DSC curves were also obtained on cooling and heating at 40 K/min. Nevertheless as those rates were not consistently kept along the corresponding ramps, the corresponding data are neither included in this Table nor were they considered for the calculation of ΔH_{av}, ΔS_{av} and N in the DSC section.

Table S2.- Selected bond angles corresponding to the HT (T=190 K) and LT phase (T=185 K) of $[(CH_3)_2NH_2][Mn(HCOO)_3]$ just above and below the structural phase transition

T=190 K		T=185K	
Bond angles (º)			
Oi-Mn-Oj	89.21(8)/ 90.79(8)	Oi-Mn-Oj	89.8(3)/ 90.5(3)/ 90.3(3)/ 88.8(3)/ 93.0(3)/ 91.1(3)/ 87.1(3)/ 89.2(2)/ 90.5(2)/ 90.1(2)
Mn-O1-C1	126.4(2)	Mn-O1-C1	129.0(6)
		Mn-O2-C3	128.8(6)
		Mn-O3-C3	126.0(6)
		Mn-O4-C4	126.6(6)
		Mn-O5-C4	124.3(6)
		Mn-O6-C1	127.9(6)
O1-C1-O1	126.2(4)	O1-C1-O6	124.8(5)
		O2-C3-O3	127.7(9)
		O4-C4-O5	126.0(8)
C2-N1-C2	118.1(8)	C21-N1-C23	110.5(8)

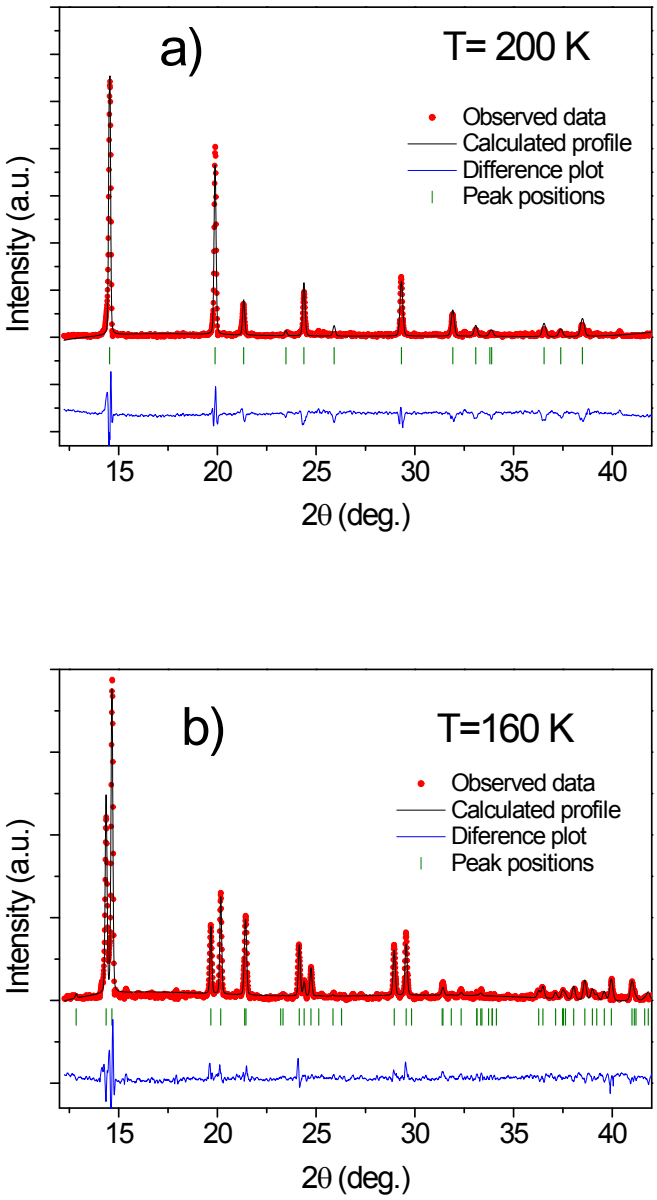

Figure S1.- LeBail refinement of powder X-ray diffraction pattern for $[(CH_3)_2NH_2][Mn(HCOO)_3]$ compound at a) T=200 K (HT-phase) and b) T=160 K (LT-phase).

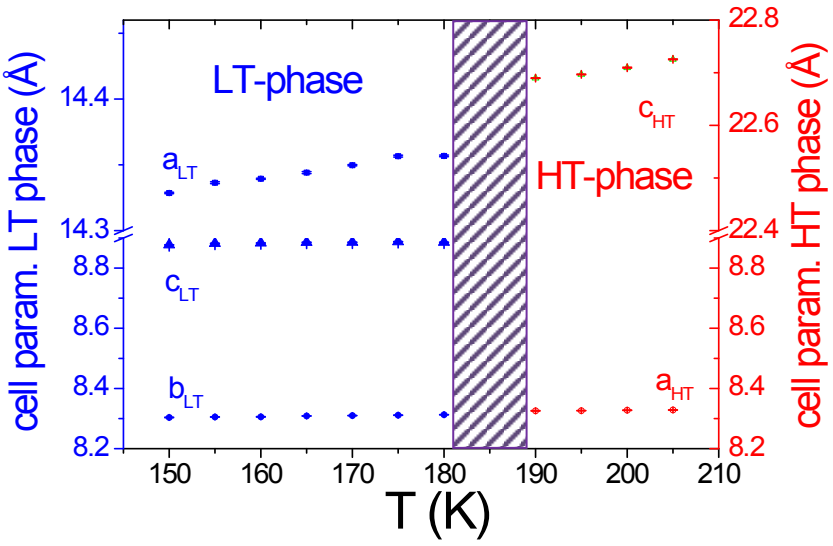

Fig. S2: Evolution of the cell parameters of the high temperature *R*-3*c* (Z=6) phase and of the low temperature *Cc* phase (Z=4) as a function of temperature.

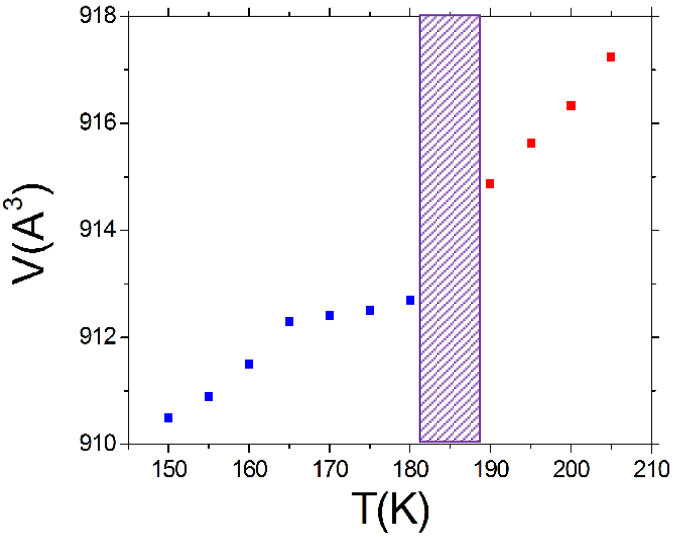

Fig. S3: Variation of the cell volume of $[(CH_3)_2NH_2][Mn(HCOO)_3]$ as a function of temperature.

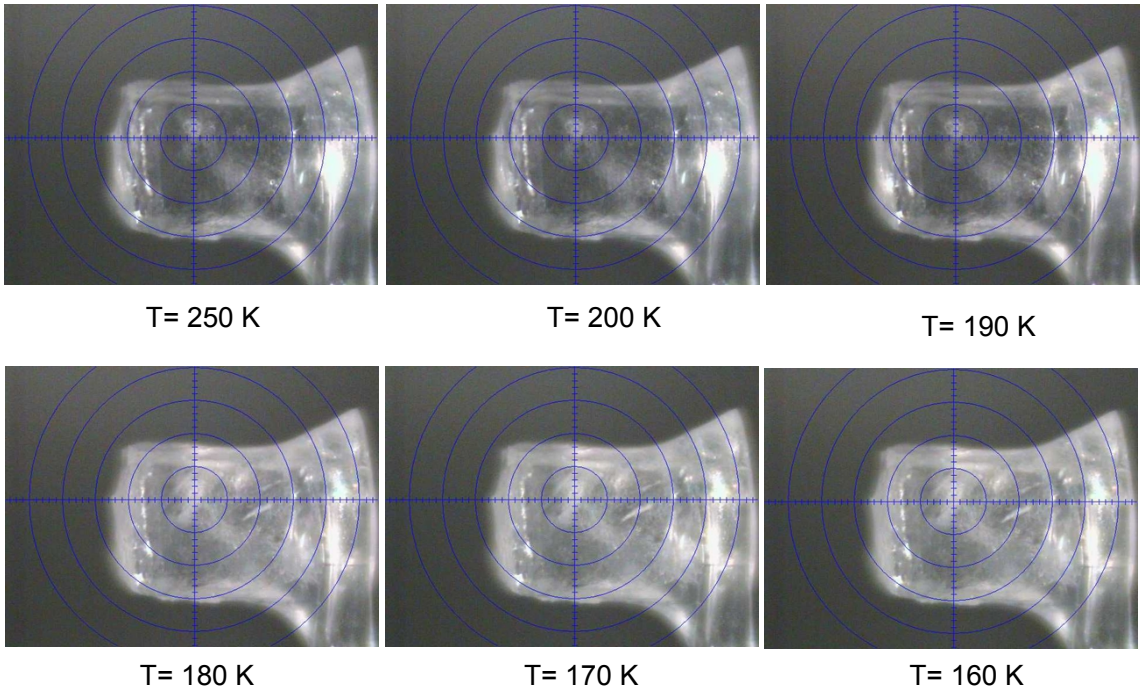

Fig. S4: Single crystal images of the $[(CH_3)_2NH_2][Mn(HCOO)_3]$ compound at different temperatures. The pictures shows as the single crystal is completely transparent at T>185 K (HT-phase) and it becomes translucent at T<185 K (LT-phase). This process is completely reversible.

Figure S5: Pseudo precession images generated from single-crystal X-ray diffraction data obtained at 185 K displaying the a) [0kl] reciprocal plane, b) [h0l] and c) [hk0] respectively. In all cases the reciprocal axes shown correspond with the first (and most populated) twin domain of the monoclinic *Cc* (LT) phase.

a)

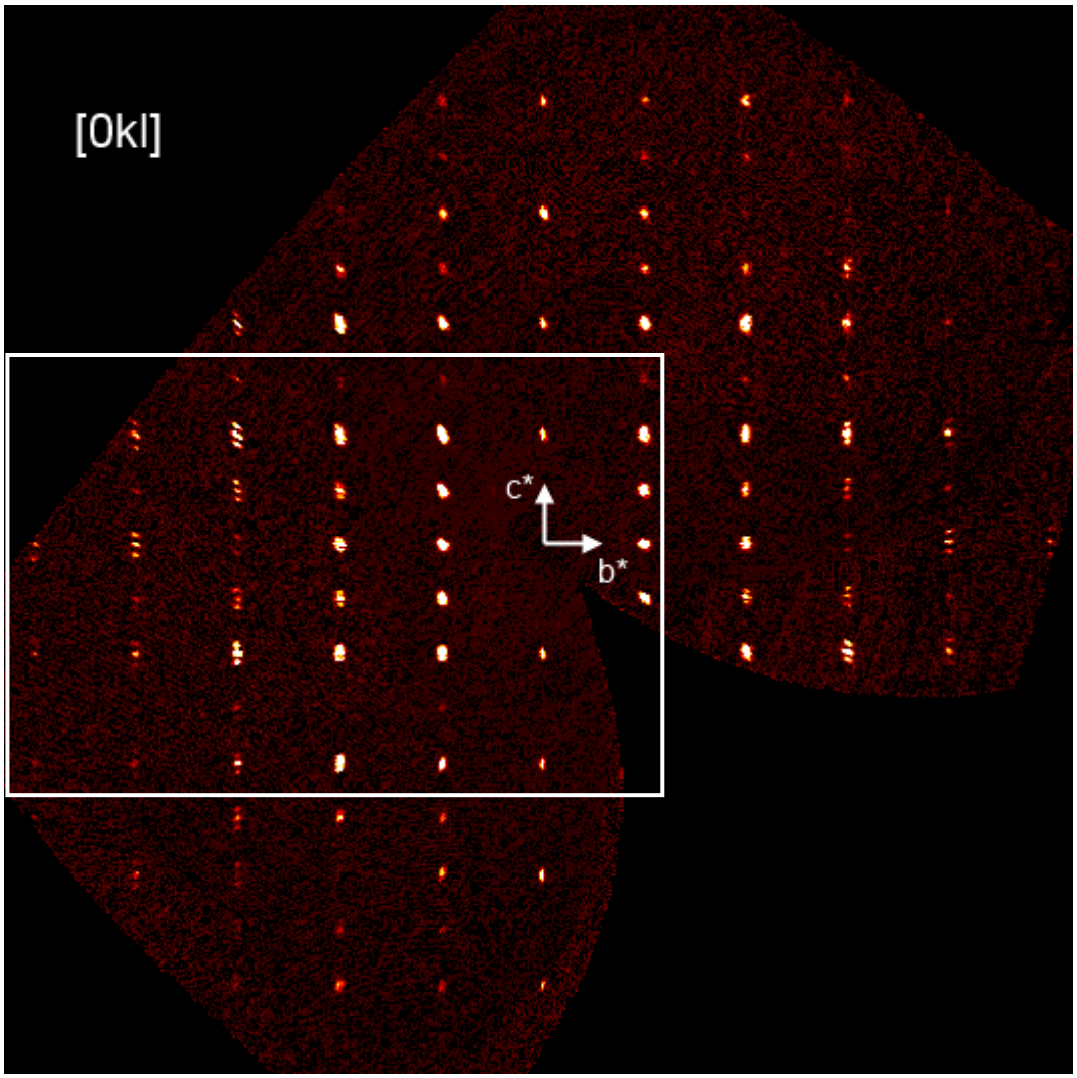

Zoom view with predicted reflections from twin domain 1, 2 and 3 respectively.

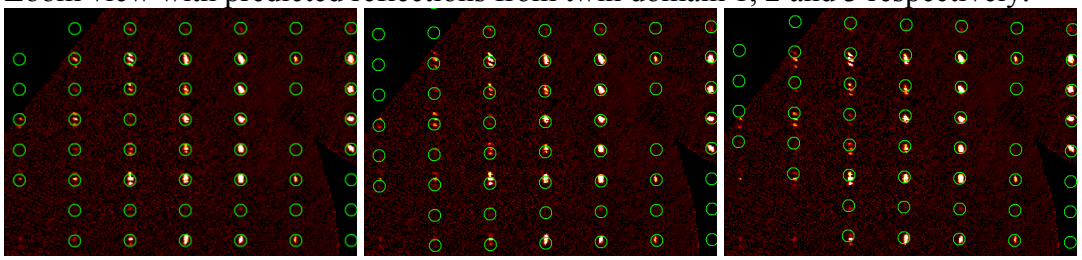

b)

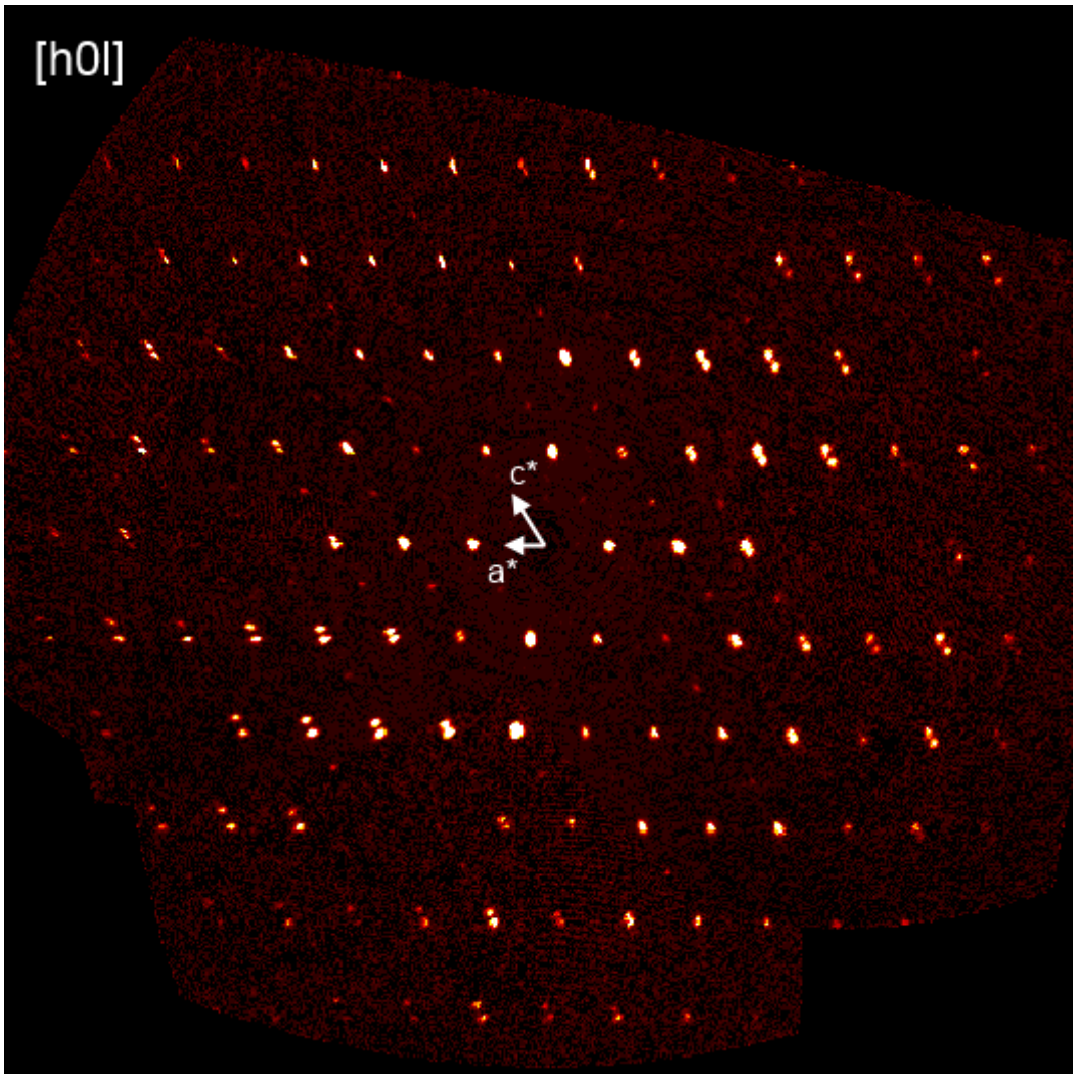

c)

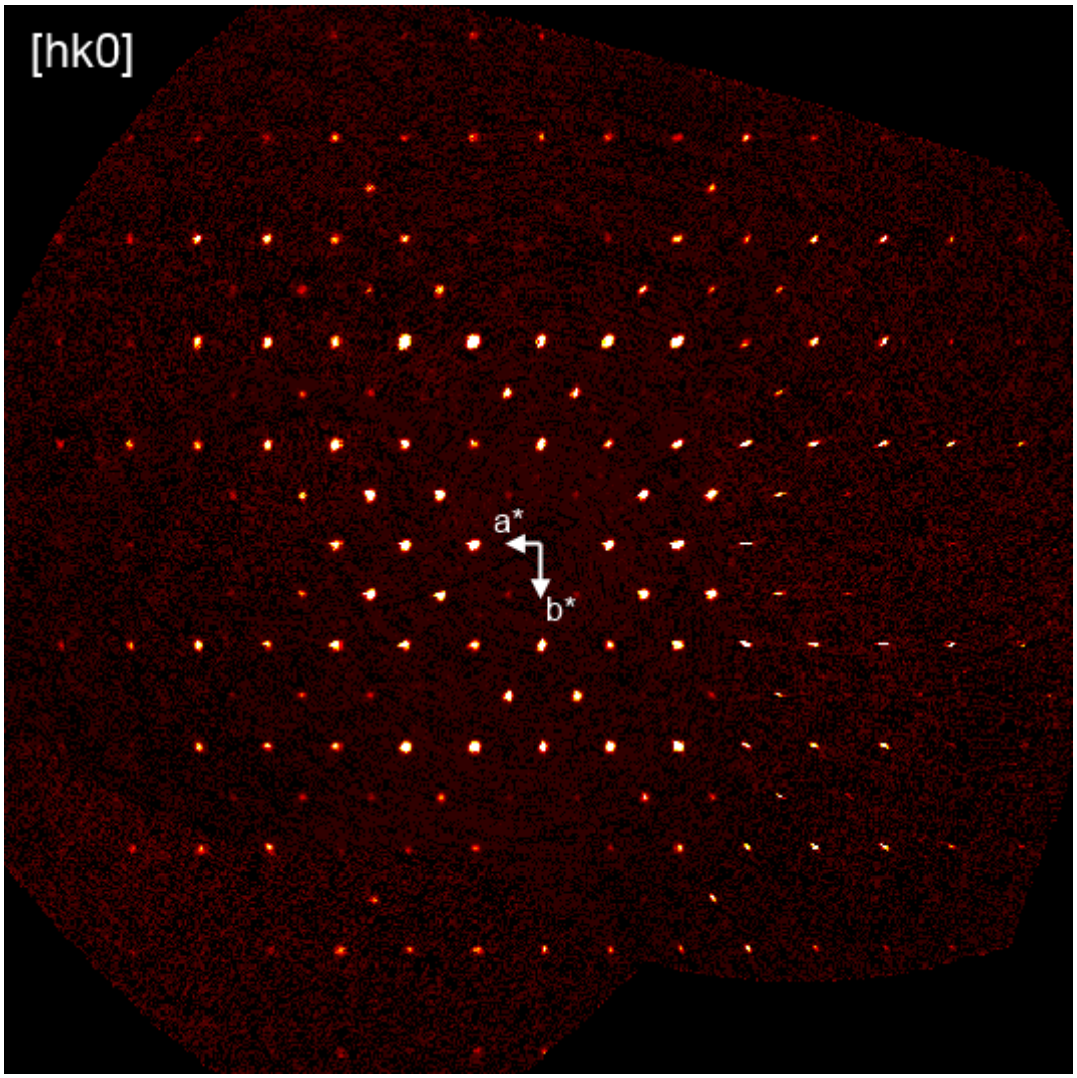

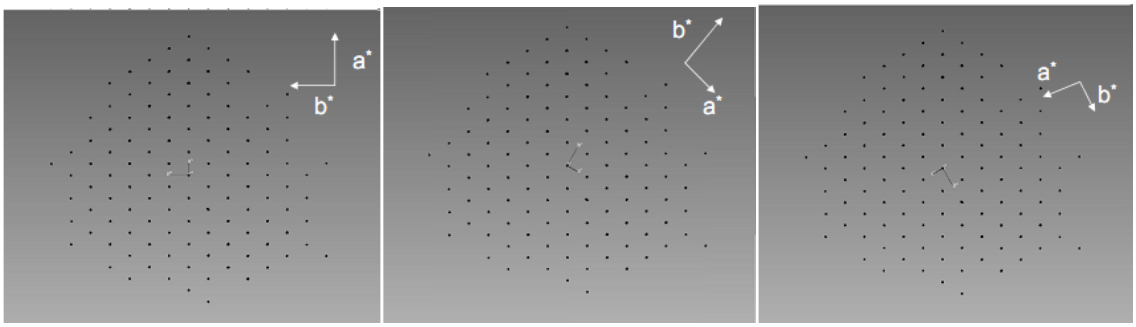

domian 1 domain 2 domain 3

Fig. S6: Projections of the reciprocal space along the c* reciprocal axis direction of the data collected at 185K (monoclinic *Cc* structure). The relative orientations of the three twin domains found is also displayed. They are related by 120º rotations around the c^* axis.

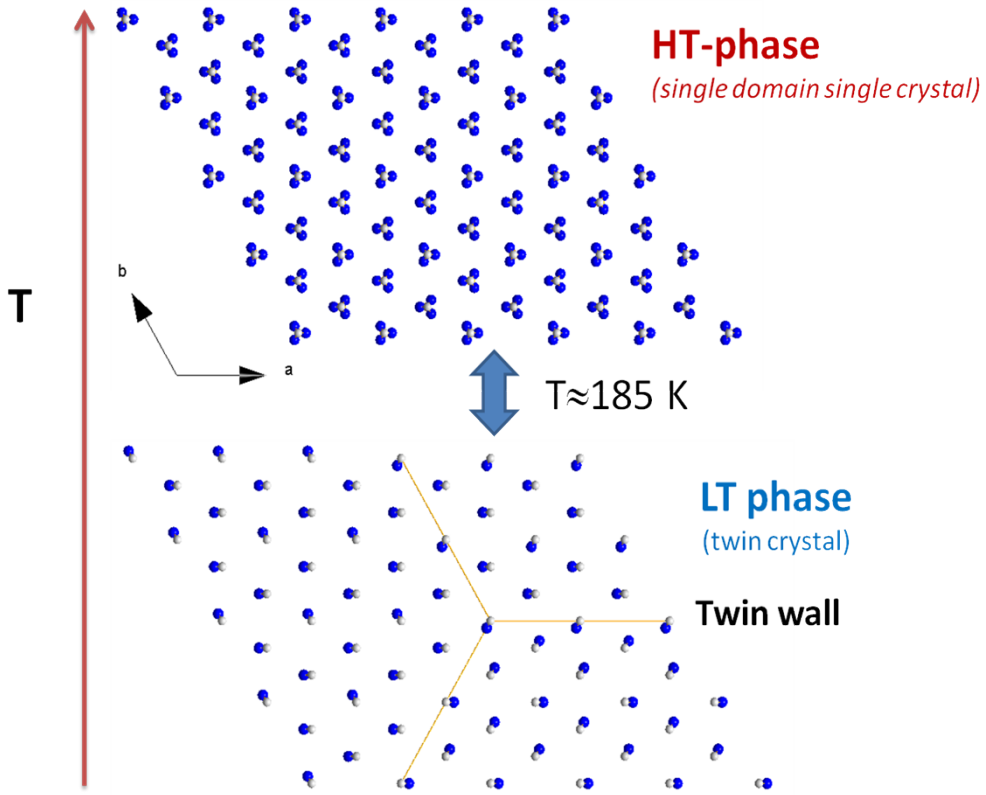

Fig. S7: Scheme of the relative orientation of the twin domains in the *Cc* monoclinic phase and its relationship to the high temperature *R*-3*c* trigonal phase. To facilitate its view, the $[Mn(HCOO)_3]^-$framework of the structure has been removed and only the DMA cations of the structure are despicted. Blue circle (N-atoms) and white circle (C-atoms) of DMA cations.